The Astrophysical Journal, 586:592–605, 2003 March 20

THE LONG-TERM EVOLUTION OF AR 7978: TESTING CORONAL HEATING MODELS

P. Démoulin,[1] L. van Driel-Gesztelyi,[1,2,3,4] C. H. Mandrini,[5,6] J. A. Klimchuk,[7] and L. Harra[3]

Received 2002 May 13; accepted 2002 November 27

ABSTRACT

We derive the dependence of the mean coronal heating rate on the magnetic flux density. Our results are based on a previous study of the plasma parameters and the magnetic flux density ($\bar{B}$) in the active region NOAA 7978 from its birth to its decay, throughout five solar rotations using the *Solar and Heliospheric Observatory* Michelson Doppler Imager, *Yohkoh* Soft X-Ray Telescope (SXT), and *Yohkoh* Bragg Crystal Spectrometer (BCS). We use the scaling laws of coronal loops in thermal equilibrium to derive four observational estimates of the scaling of the coronal heating with $\bar{B}$ (two from SXT and two from BCS observations). These results are used to test the validity of coronal heating models. We find that models based on the dissipation of stressed, current-carrying magnetic fields are in better agreement with the observations than models that attribute coronal heating to the dissipation of MHD waves injected at the base of the corona. This confirms, with smaller error bars, previous results obtained for individual coronal loops, as well as for the global coronal emission of the Sun and cool stars. Taking into account that the photospheric field is concentrated in thin magnetic flux tubes, both SXT and BCS data are in best agreement with models invoking a stochastic buildup of energy, current layers, and MHD turbulence.

Subject headings: magnetic fields — Sun: corona — Sun: magnetic fields — Sun: X-rays, gamma rays

1. INTRODUCTION

Energy is continuously supplied to the solar corona in order to maintain its temperature at more than 10^6 K. Since the major discovery of the existence of this very hot plasma in the 1940s, several mechanisms have been proposed in order to explain it. Currently, a consensus has been achieved about the origin of the energy (which is thought to be injected at the photosphere as a Poynting flux) and its mediator (namely, the coronal magnetic field). The way that this energy is dissipated in the corona is, however, still a matter of strong debate (see the variety of models summarized in § 5.2). Because of the high conductivity of the corona, an efficient way to create very fine scale lengths is required. There are several ways to induce energy dissipation at small scales (typically 10–10^3 m), so a variety of models have been proposed. However, many of the hypotheses involved in the models cannot be directly verified by observations (which have a spatial resolution larger than 10^6 m).

One test that is typically applied to models is to compare the predicted heating rate with that obtained from observations. Several models pass this test successfully for both quiet-Sun and active region (AR) conditions. Some better developed models also predict the dependence of the heating rate on parameters such as the strength of the coronal field and the length of the field lines. Mandrini, Démoulin, & Klimchuk (2000a) tested such dependence by combining the results of Porter & Klimchuk (1995), obtained for a set of 47 loops observed with the *Yohkoh* Soft X-Ray Telescope (SXT), with the magnetic extrapolations of 14 ARs. They concluded that models involving the gradual stressing of the coronal magnetic field by slow footpoint motions are generally in better agreement with the observational constraints than are wave heating models.

However, the large error bars present in the derivation of the temperature and the pressure of the set of SXT loops in Porter & Klimchuk (1995) did not allow a more stringent test of the various models. We can improve on this previous approach in three ways: first, by studying a much larger set of quiescent (nonflaring) coronal loops, second, by analyzing the long-term evolution of ARs, and finally, by using a more precise plasma diagnostic than the one provided by SXT. The aim of the present work is to follow the last two approaches. The study of the long-term evolution (decay phase) of an AR allows us to analyze a wide range of magnetic field strengths and plasma conditions. In addition, instead of following the detailed evolution of loops, we choose to analyze the global evolution of an AR not only to decrease the statistical noise but also to test the global heating of the AR. This approach is a different test from the one employed by Mandrini et al. (2000a) using the brightest loops of several ARs. This global test is more suited to some heating models. The global evolution of an AR can also be analyzed using the full-Sun *Yohkoh* Bragg Crystal Spectrometer (BCS) instrument, which provides more accurate plasma diagnostics than SXT.

Most ARs are not appropriate for the proposed study. In particular, a suitable AR should be alone on the visible disk so that BCS observations can be used, it should be observed very frequently so that flaring times can be excluded while still maintaining a large, coherent data set, and it should be observed during its entire lifetime to explore a large range of physical conditions. Moreover, it should have the simplest possible magnetic configuration while still being representative of a typical AR (magnetic flux of the order of 10^{22} Mx),

[1] Observatoire de Paris, LESIA, FRE 2461 (CNRS), F-92195 Meudon Principal Cedex, France; pascal.demoulin@obspm.fr.
[2] Centre for Plasma Astrophysics, Katholieke Universiteit Leuven, Celestijnenlaan 200B, 3001 Leuven, Belgium; lidia.vandriel@obspm.fr.
[3] Mullard Space Science Laboratory, Holmbury St. Mary, Dorking, Surrey RH5 6NT, UK; lkh@mssl.ucl.ac.uk.
[4] Konkoly Observatory, P.O. Box 67, H-1525 Budapest, Hungary.
[5] Instituto de Astronomía y Física del Espacio, IAFE, Casilla de Correos 67, Sucursal 28, 1428 Buenos Aires, Argentina; mandrini@iafe.uba.ar.
[6] Member of the Carrera del Investigador Científico, CONICET, Argentina.
[7] Naval Research Laboratory, Code 7675, Washington, DC 20375-5352; klimchuk@nrl.navy.mil.

TABLE 1
POWER-LAW DEPENDENCES

Dependent Parameter	Notation	Independent Parameter	Index	Related Equations
Radiative loss function	Λ	T	α	(2), (4)
AR area	A	$\bar{B}$	$\hat{A}$	(13)
Temperature	$\langle T\rangle_{AR}$	$\bar{B}$	$\hat{T}$	(11)
Electron density	$\langle N_e\rangle_{AR}$	$\bar{B}$	$\hat{N}$	(15)
Pressure	$\langle P\rangle_{AR}$	$\bar{B}$	$\hat{P}$	(16)
Heating rate[a] from temperature and size	$\langle H_T\rangle_{AR}$	$\bar{B}$	$\widehat{HT}$	(21), (22)
Heating rate[a] from pressure and size	$\langle H_P\rangle_{AR}$	$\bar{B}$	$\widehat{HP}$	(6), (22)
Heating rate from theoretical heating models	H_m	$\bar{B}$	$\widehat{Hm}$	(29), (30)

[a] Heating rate deduced by combining observations and the theory of coronal loops.

because heating models are basically developed for these configurations.

An AR with the above characteristics was observed during the minimum between cycles 22 and 23, from 1996 July to December. Its global evolution was analyzed in the context of the present knowledge about the long-term evolution of ARs by van Driel-Gesztelyi (1998). This region was identified as AR 7978 (NOAA number) when it first appeared on 1996 July 4 in the southern hemisphere. It was the only sizable and long-lived AR on the solar disk during five solar rotations, and so the BCS instrument could be used even during the AR decaying phase. AR 7978 had a simple bipolar magnetic configuration, which was maintained throughout its lifetime. Its magnetic flux was almost constant, but because of diffusion, its area in the photosphere increased and its magnetic field strength decreased along successive solar rotations. For these reasons, we can explore the effect of magnetic field strength on the magnitude of the coronal emission and of the coronal heating rate.

The aim of our work is to place more stringent constraints on coronal heating models than were possible in previous studies. First, we discuss the aspects of the standard theory of coronal loops in thermal equilibrium that are used to estimate the coronal heating rate (§ 2). We summarize the results of our companion paper (van Driel-Gesztelyi et al. 2003), in which we found power-law relationships between the mean coronal plasma parameters and the mean magnetic flux density ($\bar{B}$) (§ 3.1), and we test the compatibility of the thermal scaling laws with the observations of AR 7978 during its late phase (§§ 3.2 and 3.3). In § 4 we use the observational power laws and the thermal scaling laws to deduce the coronal heating rates from SXT and BCS data. Section 5 summarizes the main characteristics of the coronal heating models that predict the dependence of the heating as a function of physical parameters. Finally, we bring together all the previous results to test the present coronal heating models (§ 6), and we conclude in § 7. Since several kinds of power laws are used (deduced from observations, from the quasi-static thermal model of coronal loops, and from coronal heating models), we summarize these laws in the Appendix, and, for convenience, Table 1 lists the main power law used.

2. QUASI-STATIC THERMAL MODEL FOR CORONAL LOOPS

In this section we summarize the most important aspects of the standard theory of coronal loops in thermal equilibrium. These results are used in §§ 3 and 4.

2.1. *Basic Equations*

The basic equations are the usual magnetohydrodynamic (MHD) momentum and energy equations:

$$\rho\frac{D\boldsymbol{v}}{Dt} = -\boldsymbol{\nabla}P + \boldsymbol{j}\times\boldsymbol{B} + \rho\boldsymbol{g}\ , \tag{1}$$

$$\frac{\rho^{\gamma}}{\gamma-1}\frac{D(P\rho^{-\gamma})}{Dt} = -\boldsymbol{\nabla}\cdot\boldsymbol{F}_c - N_e^2\Lambda + H\ , \tag{2}$$

where ρ is the plasma mass density, $\boldsymbol{v}$ the plasma velocity, t the time, P the plasma pressure, $\boldsymbol{j}$ the current density, $\boldsymbol{B}$ the magnetic field, $\boldsymbol{g}$ the solar gravity, γ the ratio of specific heats, $\boldsymbol{F}_c$ the conductive flux, T the temperature, N_e the electron number density, Λ the optically thin radiative loss function, and H the volumetric heating rate.

The strong structuring of the coronal plasma by the magnetic field lets us simplify equations (1) and (2). That is, assuming a given global magnetic configuration evolving slowly with time, the plasma properties in each flux tube are nearly independent; e.g., there is negligible plasma and energy transport from one flux tube to its neighborhood. A standard procedure is then to consider equations (1) and (2) projected along magnetic field lines.

Furthermore, when the plasma velocity is smaller than the sound speed ($\approx$150 km s^{-1} for $T = 10^6$ K), the left-hand side of equation (1) is negligible (compared to the pressure gradient and gravity terms on the right-hand side). Then, the projection of equation (1) along $\boldsymbol{B}$ gives

$$\frac{dP}{ds} = -\rho g_{//}\ , \tag{3}$$

where s is the coordinate along the loop and $g_{//}$ the component of gravity along $\boldsymbol{B}$.

For most loops observed by SXT, the cooling timescale associated with radiation and thermal conduction, τ, is much shorter than the timescale for observed changes in the plasma characteristics (Porter & Klimchuk 1995; Kano & Tsuneta 1995). If the plasma velocity is lower than $2L/\tau$ (L being the half-length of the loop), the contribution to the left-hand side of equation (2) can be neglected. Such simplifications apply well to AR 7978 at times when no significant brightenings were observed with the *Geostationary Operational Environmental Satellites* (*GOES*) and SXT (van Driel-Gesztelyi et al. 2003). Finally, the thermal conduction coefficient transverse to the magnetic field is orders of magnitude lower than the parallel one. With these simplifications,

equation (2), projected along a field line, becomes

$$\frac{1}{S}\frac{d}{ds}\left(S\kappa_{//}\frac{dT}{ds}\right) = +N_e^2\Lambda(T) - H \ , \qquad (4)$$

where S is the cross-sectional area of a loop and $\kappa_{//} = \kappa_0 T^{5/2}$ is the thermal conductivity along the magnetic field. The heating function H is the major unknown of equation (4). In the simplest cases it is a function of the local plasma parameters and the magnetic field strength, but it can also depend on global quantities such as the loop length.

2.2. *Thermal Scaling Laws with Uniform Pressure*

The integration of equations (3) and (4) along a given magnetic loop gives the thermal and density structure of this loop. Starting the integration at a temperature T_0 close to a few $\times 10^4$ K (above which eq. [4] is valid), with a downward conductive flux, the temperature first rises steeply mainly because the coefficient $\kappa_{//}$ is strongly dependent on the temperature ($\propto T^{5/2}$). Then, for $T > T_c$ [with T_c defined by $N_e^2\Lambda(T_c) = H$], the temperature gradient flattens and reaches a zero value at the "top" of the loop (where $T = T_{\max}$). Because the terms in equation (4) need to balance each other, scaling laws are present. In their derivation, Rosner, Tucker, & Vaiana (1978) and Serio et al. (1981) have used a radiative cooling function $\Lambda(T) \propto T^{-1/2}$ at coronal temperatures, while Craig, McClymont, & Underwood (1978) used $\Lambda(T) \propto T^{-1}$. Vesecky, Antiochos, & Underwood (1979) and Kano & Tsuneta (1995, 1996), among others, have generalized previous works using $\Lambda(T) \propto T^{\alpha}$. The scaling laws for coronal loops in thermal equilibrium with a uniform pressure P_0 are

$$T_{\max} \propto (P_0 L)^{4/(11-2\alpha)} \ , \qquad (5)$$

$$\langle H\rangle_{\rm loop} \propto P_0^{14/(11-2\alpha)} L^{-4(2-\alpha)/(11-2\alpha)} \ , \qquad (6)$$

where we have introduced the average heating in the loop [defined by $\langle H\rangle_{\rm loop} = (\int_0^{2L} H\, ds)/(2L)$] because nonuniform heating along the loops is also considered below (see § 2.3).

It has been shown that these scaling laws are theoretically robust for loops with $T_{\max} \approx$ a few $\times 10^5$ to a few $\times 10^6$ K. In particular, they are only weakly affected by any change of the temperature ($T_0 \approx$ a few $\times 10^4$ K) or of the conductive flux F_0 at the base of the loop (provided it remains below reasonable values; see, e.g., Chiuderi, Einaudi, & Torricelli-Ciamponi 1981). A variable cross section of the loop (S) also has a small effect, even if the difference between the top and the base of the loop is an order of magnitude (e.g., Vesecky et al. 1979). Furthermore, observations show that coronal loops have a nearly constant cross section (see Klimchuk 2000 for SXT loops; Watko & Klimchuk 2000 for *Transition Region and Coronal Explorer* [*TRACE*] loops), which means that the variations in this parameter are negligible.

The scaling laws are weakly affected by the coronal exponent α of the radiative loss function [$\Lambda(T) \propto T^{\alpha}$]. Present computations of the radiative losses in optically thin plasmas indicate that α can range from -2 to $\frac{1}{3}$ depending on the temperature interval under consideration, the atomic physics included, and the elemental abundances used (Cook et al. 1989; Landi & Landini 1999). The upper ($\frac{1}{3}$) value was only found in the interval 3.6×10^6 K $\leq T \leq 8 \times 10^6$ K by Klimchuk & Cargill (2001). The effect of α is further analyzed below (§ 4).

2.3. *Generalized Thermal Scaling Laws*

There are two important effects that can modify the above scaling laws (eqs. [5] and [6]): the gravitational stratification of the coronal plasma and the spatial localization of the heating. These two effects are taken into account in the generalized scaling laws described below.

The plasma pressure decreases with height according to the integration of equation (3). This effect was first taken into account by Serio et al. (1981) in loops with a half-circular shape. These authors defined the pressure scale height according to the maximum temperature: $s_P = 2kT_{\max}/m_{\rm H}g$ ($\approx$100 Mm for $T_{\max} = 2 \times 10^6$ K). The numerical results show a small effect of this stratification on equation (5); the right-hand side is multiplied by a factor of $\exp(-0.04L/s_P)$. For a loop half-length of $L = 200$ Mm and $s_P = 100$ Mm, this gives a correction factor of $\approx$0.92. This factor is indeed an upper bound computed for the cooler and more extended portion of AR 7978 on October 23. The stratification has a much larger impact on the required heating; a factor of $\exp(-0.5L/s_P)$ multiplies the right-hand side of equation (6). We find a correction factor of 0.37 with the above numerical values.

The determination of where the heat is deposited in coronal loops can be a major constraint on coronal heating theories. However, this is difficult to infer because thermal conduction is so efficient at spreading the energy through the loop no matter where it is originally deposited (e.g., Chiuderi et al. 1981). Then, a change in the heating location implies only a small difference in the temperature profile along the loop. The most commonly used model assumes a uniform heating along the loop (see references above), but Kano & Tsuneta (1995) analyzed 16 steady SXT loops and found a temperature profile favoring the existence of a heating source at the top. Wheatland, Sturrock, & Acton (1997) arrived at basically the same conclusion for the quiet corona, except that their heating source was located at greater heights (above 0.7 $R_\odot$). This contrasts with the evidence that cooler loops (observed by *SOHO*/EIT and *TRACE*) have flat temperature profiles in favor of a heating localized in their footpoints (see Aschwanden, Schrijver, & Alexander 2001 and references therein). It is currently not known if hot loops (observed by SXT) have a fundamentally different heating input from cooler loops (observed by *SOHO*/EIT and *TRACE*), but claims for top or uniform heating in SXT loops are premature since SXT temperature profiles are indeed compatible with a wider range of models when the measurement errors are properly taken into account (Mackay et al. 2000; Reale 2002).

How do the thermal scaling laws depend on the spatial localization of the heating? Kano & Tsuneta (1995, 1996) tested the dependence of $T_{\max}$ and $\langle H\rangle_{\rm loop}$ on the heating location in two cases: the heating either is a power law of T ($H \propto T^{\beta}$) or is concentrated at the top of the loop. Both cases give the same scaling laws (only the constants in eqs. [5] and [6] are weakly affected by a factor of $\approx$1.3).

The strongest effect on the scaling laws is when the heating is localized at the base of the loops. Parameterizing the heating concentration in the loop legs as $H = H_0 \exp(-s/s_H)$ (where s_H is the scale length for the energy deposition) and using $\alpha = -0.5$ in the radiative loss function,

Serio et al. (1981) found the following scaling laws:

$$T_{\max} \propto (P_0 L)^{1/3} \exp\left(\frac{-0.08L}{s_H}\right) , \quad (7)$$

$$\langle H \rangle_{\rm loop} \propto P_0^{7/6} L^{-5/6} \frac{\sinh X}{X} , \quad (8)$$

with $X = L/2s_H$. Note that equation (8) refers to the heating rate averaged over the coronal loop and not to the heating rate at the base of the loop (H_0), as originally present in Serio et al. (1981). These results were recently confirmed by Winebarger, Warren, & Mariska (2003) and by Aschwanden et al. (2001) (to within a multiplicative factor). Both equations (7) and (8) converge to equations (5) and (6) in the limit, $s_H \gg L$, of a uniform heating (taking into account that $\alpha = -0.5$). The concentration of heating at the loop base cannot be arbitrarily large. For $s_H < L/2$, corresponding to $X > 1$, the equilibrium is unstable unless the loop has a dip at the top where the field is concave upward (Serio et al. 1981; Winebarger et al. 2003; the solutions of Aschwanden et al. 2001 differ from those of the other two studies and suggest that more severe concentrations may be possible). For the case $X = 1$, the correction to the scaling law is quite modest: $\sinh(X)/X \approx 1.17$.

By combining the corrections for pressure stratification and nonuniform heating, the scaling laws become

$$T_{\max} \propto (P_0 L)^{4/(11-2\alpha)} \exp\left[-0.04L\left(\frac{2}{s_H} + \frac{1}{s_P}\right)\right] , \quad (9)$$

$$\langle H \rangle_{\rm loop} \propto P_0^{14/(11-2\alpha)} L^{-4(2-\alpha)/(11-2\alpha)} \times \frac{\sinh X}{X} \exp\left(\frac{-0.5L}{s_P}\right) . \quad (10)$$

2.4. *Coronal Loops without Thermal Equilibrium*

Our use of equations (5), (6), (9), and (10) is only valid for loops that are in static or quasi-static equilibrium. This will be so if the heating changes slowly compared to the combined radiative and conductive cooling time or, in the case of impulsive heating, if the interval between heating episodes is short compared to the cooling time. In addition, if the heating is steady but asymmetrically distributed within the loop, steady flows will be generated, and if these flows are sufficiently fast (i.e., approach the sound speed), the scaling laws must be modified as described by Orlando, Peres, & Serio (1995a, 1995b) and Peres (2000).

Recent observations from EIT and *TRACE* indicate that many loops with temperatures near 1 MK are not in equilibrium. Some are observed to evolve rapidly, but even those that appear steady tend to have densities much higher than can be explained by equilibrium theory (e.g., Aschwanden et al. 2000). Aschwanden et al. (2001) found that about one-third of the *TRACE* loops they studied can be explained by equilibrium models if the heating is sufficiently concentrated near the footpoints, but two-thirds cannot. Winebarger et al. (2003) suggest that the fraction compatible with equilibrium may actually be smaller. On the other hand, Testa et al. (2001, 2002) have demonstrated that at least some *TRACE* loops are compatible with equilibrium models in which the coronal temperature is appreciably hotter than (≈5 MK) or cooler than (≈0.2 MK) the narrow range "allowed" by the standard *TRACE* analysis software (the software does not account for the multivalued nature of the filter ratio vs. temperature functions).

Our SXT and BCS observations are concerned with loops that are generally much hotter than 1 MK. It may very well be that these loops are fundamentally different from the loops observed by *TRACE* and EIT. In addition to being hotter (although see Testa et al. 2002), they are also broader and fuzzier in appearance, which is not an artifact of the instrumental resolution. Furthermore, there are important differences in the density properties of SXT loops. Whereas *TRACE* and EIT loops are overdense relative to equilibrium, SXT loops either have the correct density or are underdense (there is an ambiguity due to the unknown filling factor that must be assumed to convert the observed emission measure [EM] to a density). As described in Porter & Klimchuk (1995), most SXT loops are compatible with equilibrium for reasonable values of the filling factor. This is not true for *TRACE* and EIT loops, where the overdensity is exaggerated for filling factors less than 1.

Thus, while there can be no guarantee that SXT loops are in quasi-static equilibrium (see the multistrand nanoflare model of Cargill & Klimchuk 1997 and Klimchuk & Cargill 2001), the observations are consistent with such an interpretation, and so we are justified in using equations (5), (6), (9), and (10). The reader is cautioned that our analysis is probably not applicable to loops observed by *TRACE* and EIT, a majority of which are most likely not in equilibrium.

3. SCALING LAWS FOR THE CORONAL PLASMA IN AR 7978

In the present section we briefly summarize the scaling laws obtained from observations (van Driel-Gesztelyi et al. 2003), and we compare these scalings with the theoretical ones obtained for $T_{\max}$ in §§ 2.2 and 2.3.

3.1. *Summary of Previous Results*

An isolated AR (7978) was observed on the Sun during five rotations, starting in 1996 July. Because AR 7978 was nearly alone on the Sun, a large set of data from *Yohkoh*/SXT (Tsuneta et al. 1991) and *Yohkoh*/BCS (Culhane et al. 1991) is available. This data set provides a unique opportunity to study the long-term evolution of the coronal plasma as the magnetic field dispersed (van Driel-Gesztelyi et al. 2003). Using these data, together with *SOHO*/MDI longitudinal magnetograms (Scherrer et al. 1995), van Driel-Gesztelyi et al. were able to relate the plasma and the magnetic field evolutions. They selected observing periods outside any significant brightening enhancement (based on fluxes measured with *GOES* and SXT) to obtain information about the "quiet" coronal evolution.

The results of van Driel-Gesztelyi et al. (2003) are based on the analysis of *Yohkoh*/SXT partial-frame images (2.″46 pixel^{-1}). They use the filter ratio technique (Hara et al. 1992) and the GO_TEEM Solar Software (SSW) routine to compute the coronal temperature (T) and EM from the mean flux densities observed in the AlMgMn and Al.1 filters. Both T and EM are then averaged over the AR (defining $\langle T \rangle_{\rm AR}$ and $\langle {\rm EM} \rangle_{\rm AR}$). Averages over the AR are taken for three main reasons: first, to extend the study to a longer period and therefore a broader range of parameters (individual loops are discernible only in the early period), second, to analyze the full coronal plasma of the AR, and

finally, to have a closer comparison with BCS results. BCS temperatures and EMs were estimated using the FIT_BCS spectral fitting routine within the SSW analysis system. The S XV line complex was analyzed with the software written by D. Zarro and J. Lemen, which uses a minimization χ^2 technique. The average magnetic flux density $\bar{B}$ (magnetic flux divided by the photospheric area of the AR) was derived from the longitudinal magnetograms of *SOHO*/MDI. Further information can be found in van Driel-Gesztelyi et al. (2003).

The main results of van Driel-Gesztelyi et al. can be summarized as follows: The mean temperature and mean EM derived from both SXT and BCS, as well as the SXT fluxes in both the Al.1 and AlMgMn filters, are well described by power laws of the average magnetic flux density $\bar{B}$:

$$\langle T\rangle_{\rm AR} \propto \bar{B}^{\hat{T}} \ , \tag{11}$$

$$\langle {\rm EM}\rangle_{\rm AR} \propto \bar{B}^{\widehat{\rm EM}} \ . \tag{12}$$

The dependence on $\bar{B}$ holds throughout the long-term evolution of the AR, including both the emerging phase, in which $\bar{B}$ increases, and the decaying phase, in which $\bar{B}$ decreases.

The AR area A, defined by the photospheric magnetic extension of the region, was also found to have a power-law dependence on $\bar{B}$:

$$A \propto \bar{B}^{\hat{A}} \ , \tag{13}$$

where $\hat{A} \approx -1.0$, indicating that magnetic flux is approximately constant. The coronal loops expand as the AR photospheric magnetic field becomes more extended. We assume that the half-length L of coronal loops scales with the AR horizontal extension:

$$L \propto \sqrt{A} \propto \bar{B}^{\hat{A}/2} \ . \tag{14}$$

The EM of the AR at the limb has been found to decrease exponentially with height with a scale height proportional to $\sqrt{A}$ (see the appendix of van Driel-Gesztelyi et al. 2003 for further justifications). Then equations (12) and (14) can be combined to give a power law for the electron density:

$$\langle N_e\rangle_{\rm AR} \propto \bar{B}^{\hat{N}} \ . \tag{15}$$

Equation (15) can then be combined with equation (11) and the ideal gas law to get

$$\langle P\rangle_{\rm AR} \propto \bar{B}^{\hat{P}} \ . \tag{16}$$

Table 1 lists the physical parameters and power-law exponents of these various scaling laws as well as other scaling laws that we introduce below. The scaling laws are also summarized in the Appendix.

Two different statistical methods were used to determine the values of the power-law exponents from the observations: a standard method that is valid when the data are normally distributed (i.e., follow a Gaussian distribution) and a nonparametric method that has more general application. The results are summarized in Figure 1. The error range quoted for the Gaussian method is $\pm 3\ \sigma$, which corresponds to a 99% confidence interval. The error range quoted for the nonparametric method corresponds to a 90% confidence interval and, because it is not necessarily symmetric around the most probable value (see the discussion in Porter & Klimchuk 1995), is indicated slightly differently with $\pm$ notation.

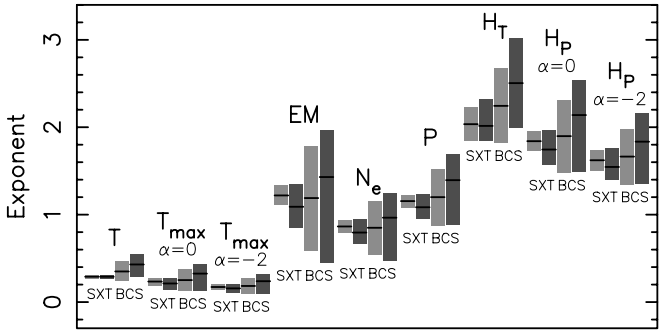

FIG. 1.—Ranges for the exponents found for the mean physical parameters in the scaling law equations: parameter $\propto \bar{B}^{\rm exponent}$ ($\bar{B}$: magnetic flux density). The temperature T and the EM are derived directly from the observations, and then the plasma density N_e and pressure P are deduced (see § 3.1). The quantity $T_{\rm max}$ is the maximum temperature derived from the quasi-static thermal model of coronal loops (§§ 3.2 and 3.3). Quantities H_T and H_P are the heating rates derived from the observations and the thermal model (§ 4). For $T_{\rm max}$ and H_P, two values of α are shown (coronal radiative losses $\propto T^{\alpha}$). The $\pm 3\ \sigma$ error range (99% confidence interval) of normally distributed statistics is light shaded. The confidence interval of the nonparametric statistics is dark shaded (90% confidence interval for SXT; see van Driel-Gesztelyi et al. 2003 for BCS).

3.2. *Test of the Scaling Law Using SXT*

To test the scaling predicted by equation (5) for thermal equilibrium, we use equation (14), and we assume that $\langle P\rangle_{\rm AR}$ gives a good proxy for the dependence of the pressure P_0 at the base of the loops. This is likely, since the effect of the gravitational stratification is not so important (van Driel-Gesztelyi et al. 2003). Moreover, the test provided by equation (5) is meaningful because the product P_0L has a significant dependence on $\bar{B}$ ($P_0L \propto \bar{B}^{0.64\pm0.10}$ and $P_0L \propto \bar{B}^{0.59^{+0.19}_{-0.17}}$).

Combining the SXT results of van Driel-Gesztelyi et al. (2003) for equations (16) and (13) with the theoretical scaling law of equation (5), we then obtain

$$\begin{aligned} T_{\rm max} &\propto (P_0L)^{0.36} \text{ for } \alpha = 0 \ , \\ &\propto \bar{B}^{0.23\pm0.04} \text{ or } \bar{B}^{0.21^{+0.06}_{-0.07}} \ , \end{aligned} \tag{17}$$

$$\begin{aligned} T_{\rm max} &\propto (P_0L)^{0.27} \text{ for } \alpha = -2 \ , \\ &\propto \bar{B}^{0.17\pm0.03} \text{ or } \bar{B}^{0.16^{+0.05}_{-0.05}} \ , \end{aligned} \tag{18}$$

using two values of α from the radiation law. Although $T_{\rm max}$ and $\langle T\rangle_{\rm AR}$ refer to the maximum and average temperatures in the loops, respectively, detailed equilibrium models show that these two temperatures are closely related (J. A. Klimchuk 2003, in preparation), so a direct comparison is appropriate. The exponents of $T_{\rm max}$ are relatively close to those found from observations alone: $\langle T\rangle_{\rm AR} \propto \bar{B}^{0.29\pm0.02}$ and $\langle T\rangle_{\rm AR} \propto \bar{B}^{0.29^{+0.02}_{-0.02}}$ (see the comparison in Fig. 1). However, there is an agreement within the error bars of both statistics only when $\alpha \gtrsim 0$. We conclude that the scaling law of $T_{\rm max}$ (deduced assuming thermal equilibrium) is only partially in agreement with the scaling law of $\langle T\rangle_{\rm AR}$ derived solely from

the observations. This may have an origin in the hypothesis made, and/or we may have underestimated the error bars and/or included systematic errors.

3.3. *Test of the Scaling Law Using BCS*

We have made a similar comparison using the BCS results from van Driel-Gesztelyi et al. (2003):

$$T_{\max} \propto \bar{B}^{0.25\pm0.12} \text{ for } \alpha = 0 \ , \quad \text{or } \bar{B}^{0.33^{+0.11}_{-0.19}} \ , \tag{19}$$

$$T_{\max} \propto \bar{B}^{0.18\pm0.09} \text{ for } \alpha = -2 \ , \quad \text{or } \bar{B}^{0.24^{+0.08}_{-0.14}} \ . \tag{20}$$

The upper end of the 90% confidence interval is not well defined in the nonparametric analysis of these data, and the values quoted correspond to 59% and 82% confidence levels in temperature and EM, respectively. Both $\langle T \rangle_{\rm AR}$ and $T_{\max}$ exponents are slightly higher with BCS than with SXT (Fig. 1). For BCS, these exponents are fully compatible, within the confidence interval, for both statistics and for the entire coronal range of α [$-2.$, 0.33].

3.4. *Comparison with Other Estimations*

The test of the scaling predicted by equation (5) has also been done by other authors using SXT. The closest approach to ours is that of Yashiro & Shibata (2001), who considered average quantities for 64 ARs. They found $\langle T \rangle_{\rm AR} \propto (P_0 L)^{0.34\pm0.08}$, a scaling fully compatible with equation (5).

For studies considering a set of loops, therefore a priori more appropriate to test equation (5), the results are contradictory. Porter & Klimchuk (1995) analyzed the relationship of the loop length with the temperature and the pressure for 47 quasi-static loops. Their results are compatible, within the error bars, with equation (5) for any α-value, since they found $P_0 \propto L^{-1}$ and $T_{\max}$ independent of L. However, Kano & Tsuneta (1995) found for another set of 32 quiescent loops a deviation from equation (5): $T_{\max} \propto (P_0 L)^{0.2\pm0.02}$ (which would imply $\alpha \approx -4.5$!). In our case, we rather find a larger exponent: $\langle T \rangle_{\rm AR} \propto (P_0 L)^{0.45\pm0.09}$ or $(P_0 L)^{0.50^{+0.17}_{-0.15}}$ with SXT and $\langle T \rangle_{\rm AR} \propto (P_0 L)^{0.51\pm0.29}$ or $(P_0 L)^{0.48^{+0.32}_{-0.23}}$ with BCS. Most of these exponents are slightly above the exponent predicted by equation (5): $4/(11 - 2\alpha)$ (=0.39 for $\alpha = 0.33$, 0.36 for $\alpha = 0$, and 0.27 for $\alpha = -2$).

4. SCALINGS OF THE HEATING RATE DEDUCED FROM OBSERVATIONS

4.1. *How Can Heating Scaling Laws Be Deduced from Observations?*

The thermal scaling laws introduce the loop half-length (L) and the base pressure (P_0) (or the maximum temperature $T_{\max}$) as the main parameters, which determine the average heating rate ($\langle H \rangle_{\rm loop}$) as summarized in § 2. It is then natural to apply these scaling laws to individual coronal loops to test the coronal heating models (Mandrini et al. 2000a). We follow here a global approach for three reasons: first, because the loop approach cannot be applied to BCS data; second, because when it can be applied (SXT), it is only to a limited number of coronal loops so that all the information in the surrounding plasma is discarded; and finally, because we want to test the coronal heating models in a different way from Mandrini et al. (2000a). This global approach allows us to reduce the statistical errors due to photon noise, especially when the AR loops are faint and the magnetic field has evolved into an enhanced network-like field.

The scaling laws determined for AR 7978 by van Driel-Gesztelyi et al. (2003) show that the plasma characteristics are linked to the magnetic flux density $\bar{B}$ of the AR via power laws (see the summary in § 3.1). Below, we use these observed relationships to deduce the scaling law of the coronal heating rate versus $\bar{B}$. The averaged coronal heating can be computed, in general, from equation (10) (or as a function of $T_{\max}$ using eq. [9]). However, as discussed below, we believe it is sufficient to use the simpler expressions given in equations (5) and (6).

First, there is no observational evidence that the plasma stratification by gravity plays a significant role in the observed average values (van Driel-Gesztelyi et al. 2003). Moreover, this gravitational stratification is not taken into account in present models of coronal heating (§ 5).

Second, evidence of a strongly concentrated heating low in the loop legs is present only for about one-third of UV loops (Aschwanden et al. 2001). For hot coronal loops, observations cannot clearly distinguish between a moderate concentration in the legs, a uniform heating, or a top heating (Mackay et al. 2000; Reale 2002). For these three distributions, the average heating deduced from equation (10) is not sensitive to the location of the heat source. Furthermore, even if the heating were strongly concentrated in the loop legs, the scaling law would not be affected in the AR average as long as the ratio $X = L/2s_H$ was statistically independent of loop length (but this would introduce a larger dispersion in the observed results).

For these reasons, we use below the scaling laws given by equations (5) and (6), rather than the more general ones given by equations (9) and (10).

4.2. *Derivation of the Heating Rate from Observations*

Observations provide two nearly independent quantities: plasma temperature and EM. From these quantities we obtain plasma temperature and pressure that are only partially correlated (the pressure scaling depends more on the EM than on the temperature scaling). Then, we can calculate the average heating as a function of the pressure (eq. [6]) or as a function of the temperature by eliminating the pressure between equations (5) and (6):

$$\langle H \rangle_{\rm loop} \propto T_{\max}^{7/2} L^{-2} \ . \tag{21}$$

The right-hand side is roughly proportional to the thermal conduction cooling rate averaged over the loop. Equation (21) indicates that thermal conduction cooling and, therefore, also radiation cooling are approximately fixed fractions of the heating, independent of the details of the radiation law (i.e., the value of α). Furthermore, radiation and conduction are of comparable magnitude, so neither fraction is especially small (e.g., Vesecky et al. 1979; J. A. Klimchuk 2003, in preparation).

Van Driel-Gesztelyi et al. (2003) have found that the mean temperature and pressure scale with the magnetic flux

TABLE 2
EXPONENTS IN THE POWER-LAW FUNCTION OF THE HEATING

Heating Deduced from:	Notation	Instrument	Gaussian Exponent	Nonparametric Exponent
Temperature and size	$\widehat{HT}$	SXT	2.03 ± 0.19	$2.01^{+0.31}_{-0.17}$
Pressure and size	$\widehat{HP}$	SXT	1.84 ± 0.11	$1.74^{+0.22}_{-0.17}$
Temperature and size	$\widehat{HT}$	BCS	2.24 ± 0.42	$2.51^{+0.52}_{-0.51}$
Pressure and size	$\widehat{HP}$	BCS	1.90 ± 0.42	$2.14^{+0.40}_{-0.65}$

NOTES.—Exponents $\widehat{HT}$ and $\widehat{HP}$ in the power-law functions $\langle H_T \rangle_{\rm AR} \propto \bar{B}^{\widehat{HT}}$ and $\langle H_P \rangle_{\rm AR} \propto \bar{B}^{\widehat{HP}}$ for the heating rate per unit volume as a function of the magnetic flux density ($\bar{B}$), as derived in § 4 (computed for $\alpha = 0$). The results with normally distributed (Gaussian) statistics and with nonparametric statistics are given with a $\pm 3\,\sigma$ error range (99% confidence interval) and with a 90% confidence interval as $\pm$ (see van Driel-Gesztelyi et al. 2003 for BCS).

density: $\langle T \rangle_{\rm AR} \propto \bar{B}^{\hat{T}}$ and $\langle P \rangle_{\rm AR} \propto \bar{B}^{\hat{P}}$. We use equation (14) for the loop half-length and $\langle T \rangle_{\rm AR}$ and $\langle P \rangle_{\rm AR}$ as proxies for $T_{\rm max}$ and P_0. With these hypotheses, equations (21) and (6) give two scalings for the coronal heating averaged over the AR (see Table 2):

$$\langle H_T \rangle_{\rm AR} \propto \bar{B}^{\widehat{HT}} \ ,$$
$$\langle H_P \rangle_{\rm AR} \propto \bar{B}^{\widehat{HP}} \ , \tag{22}$$

with

$$\widehat{HT} = \tfrac{7}{2}\hat{T} - \hat{A} \ , \tag{23}$$
$$\widehat{HP} = \frac{14\hat{P} + 2(\alpha - 2)\hat{A}}{11 - 2\alpha} \ . \tag{24}$$

The exponent $\widehat{HP}$ has a weak dependence on α. Because the present knowledge of the coronal radiative losses favors higher values of α in the range of temperatures observed by SXT and BCS (e.g., Klimchuk & Cargill 2001) and because the temperature scaling law (eq. [5]) is better satisfied with such higher values (see §§ 3.2 and 3.3), we mainly use $\alpha = 0$ below (unless specified otherwise). The slight shift of $\widehat{HP}$ for lower α's can be deduced taking into account that this shift is approximately linear in α. The cases $\alpha = 0$ and -2 shown are in Figures 1, 2, and 4.

4.3. *Results Using SXT*

We find for the two statistics (and $\alpha = 0$ for $\widehat{HP}$)

$$\widehat{HT}_{\rm SXT} = 2.03 \pm 0.19 \ ,$$
$$\text{or } 2.01^{+0.31}_{-0.17} \ , \tag{25}$$
$$\widehat{HP}_{\rm SXT} = 1.84 \pm 0.11 \ ,$$
$$\text{or } 1.74^{+0.22}_{-0.17} \ . \tag{26}$$

Such close agreement between $\widehat{HP}_{\rm SXT}$ and $\widehat{HT}_{\rm SXT}$ was not obvious a priori, even considering our selection of periods without flaring, because we have transformed the scaling laws obtained for individual loops to scaling laws for the full AR. Our global approach combines loops with different temperatures and EMs. Only averages are obtained, and the details of the averaging (e.g., temperature weighting) are determined by the instrument and the type of observed solar features. The success of this global approach probably resides in the power-law dependence of all the plasma quantities on the magnetic field strength.

4.4. *Results Using BCS*

From BCS results (and $\alpha = 0$ for $\widehat{HP}$), we find

$$\widehat{HT}_{\rm BCS} = 2.24 \pm 0.42 \ ,$$
$$\text{or } 2.51^{+0.52}_{-0.51} \ , \tag{27}$$
$$\widehat{HP}_{BCS} = 1.90 \pm 0.42 \ ,$$
$$\text{or } 2.14^{+0.40}_{-0.65} \ . \tag{28}$$

The exponents $\widehat{HT}_{\rm BCS}$ and $\widehat{HP}_{\rm BCS}$ are only slightly higher than $\widehat{HT}_{\rm SXT}$ and $\widehat{HP}_{\rm SXT}$ but compatible within the confidence intervals. Since the biases in SXT data are of a different nature from those in BCS, the closeness between these exponents is remarkable. The fact that, with both SXT and BCS, we have found slightly lower exponents when using the mean pressure than when using the mean temperature may imply the existence of an intrinsic bias (directly linked to the difference in scaling found between $T_{\rm max}$ and $\langle T \rangle_{\rm AR}$ in §§ 3.2 and 3.3). Still, the main result here is that scaling laws of the coronal heating with the magnetic field can be determined accurately enough to test present heating models. The compatibility of the four exponents $\widehat{HT}_{\rm SXT}$, $\widehat{HT}_{\rm BCS}$, $\widehat{HP}_{\rm SXT}$, and $\widehat{HP}_{\rm BCS}$ strengthens this conclusion.

5. CORONAL HEATING MODELS

5.1. *Scaling of the Heating Deduced from Models*

Most coronal heating models give a heating rate per unit volume that can be expressed in the following generic way:

$$H_m \propto B^a L^b N_e^c V^d R^e \ , \tag{29}$$

where B is the coronal field strength, L is the loop length, N_e is electron density, V is the transverse (horizontal) velocity at the base of the corona, and R is the loop radius or the transverse scale length for the magnetic or flow field, depending on the model. The coefficients a through e predicted by a variety of models are given in Table 5 of Mandrini et al. (2000a).

As a proxy of the coronal field B, we use the photospheric flux density $\bar{B}$. If we know how L, N_e, V, and R depend on $\bar{B}$, then equation (29) can be written as

$$H_m \propto \bar{B}^{\widehat{Hm}} \ , \tag{30}$$

where the exponent $\widehat{Hm}$ is model dependent. Such a power-law function is indeed justified by observations (§ 4), and the comparison of $\widehat{Hm}$ with $\widehat{HP}$ and $\widehat{HT}$ lets us test the various models.

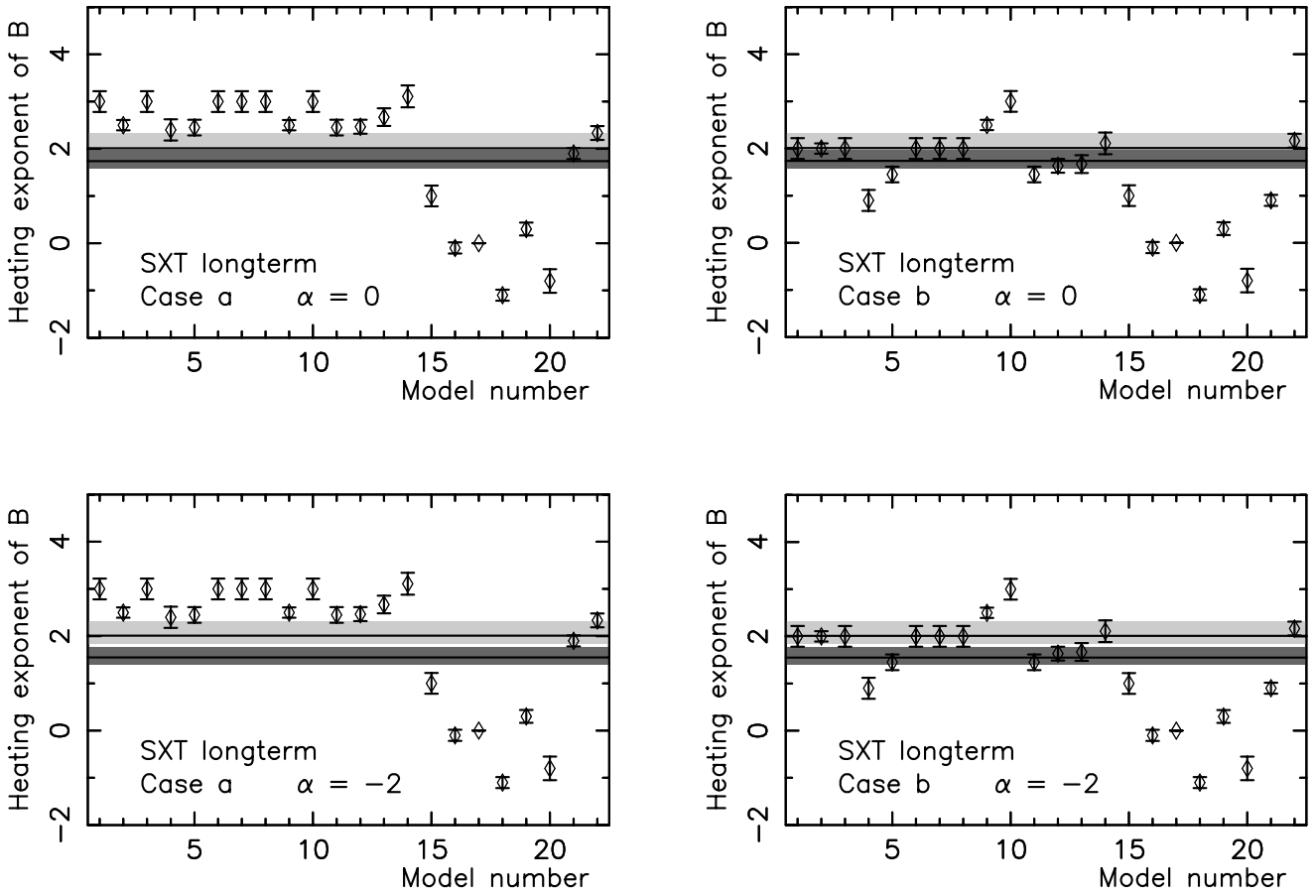

FIG. 2.—Comparison of the heating rate $\langle H \rangle$ vs. magnetic flux density $\bar{B}$ scaling law, $\langle H \rangle \propto \bar{B}^{\tilde{H}}$, as deduced from observations and models. We show the case for α (exponent for the coronal radiative losses expression) $=0$ (*top*) and -2 (*bottom*). The horizontal lines are the two most probable values of the exponents $\widetilde{HT}$ and $\widetilde{HP}$ as deduced from the thermal scaling laws and from the long-term study of AR 7978 with SXT and MDI using a nonparametric fit (§ 4.3, Table 2). The darker and lighter gray regions indicate the 90% confidence interval deduced from the measured mean pressure and temperature, respectively. See Fig. 1 to better compare the ranges found for $\widetilde{HT}$ and $\widetilde{HP}$. The plotted points with error bars indicate the power-law index $\widetilde{Hm}$ predicted by the models summarized in § 5.2 (the scaling laws are given in Table 5 of Mandrini et al. 2000a). Case *a* represents the original model prediction (with a nearly uniform large-scale magnetic field), and case *b* takes into account a correction coming from the concentration of the photospheric magnetic field in thin flux tubes when twisting motions are involved (see § 5.1).

The dependence of L on $\bar{B}$ is expressed by equation (14). The N_e dependence has been determined from observations by van Driel-Gesztelyi et al. (2003). This leaves V and R. These parameters refer to the base of the corona, which is separated from the photosphere by the chromosphere and transition region. How are V and R related in these two regions? Since most models have not taken into account this difficulty, we adopt two extreme cases as done in Mandrini et al. (2000a). One possibility, which we refer to as case *a*, is that the coronal and photospheric quantities are identical:

$$R = R_{\rm ph} \ , \quad V = V_{\rm ph} \quad (\text{case } a) \ . \tag{31}$$

This is the assumption made for nearly all published models, which is valid mainly for braiding or shearing motions. A second possibility, case *b*, takes into account the well-known fact that the photospheric field is strongly concentrated in thin flux tubes. For twisting motions, magnetic flux and angular velocity conservation imply (van Ballegooijen 1986)

$$R \approx R_{\rm ph} \sqrt{\frac{B_{\rm ph}}{B}} \ , \quad V \approx V_{\rm ph} \sqrt{\frac{B_{\rm ph}}{B}} \quad (\text{case } b) \ . \tag{32}$$

If we further assume that the local photospheric quantities $B_{\rm ph}$, $R_{\rm ph}$, and $V_{\rm ph}$ are statistically independent of the coronal field B, then case *b* has an additional contribution $\bar{B}^{-(d+e)/2}$ in H_m, when compared to case *a*.

5.2. *An Overview of Coronal Heating Models*

Models or theories of coronal heating can be divided into two main categories: stressing (or direct current [DC]) models and wave (or alternating current [AC]) models. The main difference is the ratio between the timescale of the motions imposed at the base of a loop and the time it takes an Alfvén wave to cross that loop. When this ratio is larger than unity, DC heating dominates, while for a ratio smaller than unity, AC heating dominates. In the DC models, photospheric and subphotospheric motions displace the field line footpoints in both random and systematic ways and can include both translational and rotational components. The magnetic free energy that is pumped into the field can be released in real time or stored in the field to be released later. Thus, the resulting plasma heating can be steady, quasi-steady, or highly episodic depending on the model. In AC models, MHD waves are generated at the base of the corona, possibly by photospheric turbulence, and propagate upward to

heat the corona. Although waves can be generated directly in the corona as a by-product of bursty reconnection, we classify that situation as DC heating, since the energy that powers the waves resides initially in the stressed coronal magnetic fields. We now describe briefly a series of different models that we number in the same way as in Table 5 of Mandrini et al. (2000a).

1. Stressing models:

Stochastic buildup.—Models 1 (Sturrock & Uchida 1981; Berger 1991) and 3 (Galsgaard & Nordlund 1997) consider the photospheric forcing of the coronal field by the random twisting of individual flux tubes, while model 2 (Parker 1988; Berger 1993) considers the braiding of flux tubes. In model 2, energy release occurs when a critical angle is reached between adjacent misaligned flux tubes, while in model 3, it occurs when a critical twist is reached.

Reconnection.—Models 4 (Parker 1983) and 5 explicitly involve magnetic reconnection. Model 5 is a modification of Parker's original derivation to account for the fact that the reconnection rate is likely to depend on the transverse field strength, rather than on the total field strength (see Mandrini et al. 2000a).

Current layers.—Models 6–8 (van Ballegooijen 1986; Hendrix et al. 1996; Galsgaard & Nordlund 1996) involve the exponential growth of concentrated currents induced by continuous footpoint motions.

Current sheets.—Model 9 (Aly & Amari 1997) considers the formation and destruction of true current sheets in magnetic configurations containing X-points. We have found that the scaling of this model is not correct in Table 5 of Mandrini et al. (2000a), since it should not depend on R.

Taylor relaxation.—Model 10 (Heyvaerts & Priest 1984; Browning & Priest 1986; Vekstein, Priest, & Steele 1993) makes use of Taylor's conjecture (Taylor 1974) that the magnetic field relaxes via reconnection to the lowest energy state that preserves helicity.

Turbulence.—In models 11–14 (Einaudi et al. 1996; Dmitruk & Gómez 1997; Heyvaerts & Priest 1992; Inverarity, Priest, & Heyvaerts 1995; Inverarity & Priest 1995a; Milano, Gómez, & Martens 1997), energy is pumped into the field at large scales, and it cascades to smaller scales, at which it is dissipated. The models differ from one another in the way the nonlinearities are treated in the MHD equations.

2. Wave models:

Resonance.—Models 15 and 16 (Hollweg 1985) addresses the conditions that have to be met in order for significant MHD wave energy to be transmitted into the loop from below.

Resonant absorption.—Models 17–20 (Ofman, Davila, & Steinolfson 1995; Ruderman et al. 1997; Halberstadt & Goedbloed 1995) consider a different aspect of loop resonance: the amplification of the wave amplitude in a narrow layer where the local Alfvén resonance frequency matches the frequency of the global loop oscillations.

Current layers.—Model 21 (Galsgaard & Nordlund 1996) is basically the same as model 8, but taken in the limit of rapid boundary excitations compared to the end-to-end Alfvén travel time.

Turbulence.—Model 22 (Inverarity & Priest 1995b) is similar to model 12, except that the footpoint motions have a high enough frequency to produce waves rather than a quasi-static evolution.

A more extended description of the models is presented in Mandrini et al. (2000a). The heating rate derived by these models can be expressed in the generic way of equation (29), as summarized in their Table 5. Some models depend on extra parameters, which are assumed to be independent of $\bar{B}$. One main parameter for the AC models is the slope m assumed for the frequency spectrum of the driver ($\propto \omega^m$). Since this parameter is not known, we consider three possible values: $m = -1$ for models 13, 15, 17, and 19, $m = -2.5$ for model 14, and $m = -2$ for models 16, 18, and 20.

Recently, a new model was proposed by Sturrock, Roald, & Wolfson (1999) and developed by Roald, Sturrock, & Wolfson (2000). The coronal heating of the quiet Sun is suggested to come from chromospheric reconnection between flux tubes mainly in the supergranule network. At first, we may think that this model could be applied to ARs in their decaying phase, since their photospheric field is progressively transformed to an enhanced network (van Driel-Gesztelyi 1998). However, the model relies on the assumption of magnetic neutrality, which is not satisfied in both polarities of AR 7978. Moreover, Pevtsov & Acton (2001) found no correlation between the soft X-ray emission and the local mean field of the quiet Sun, in contradiction with the model of Sturrock et al. (1999). Therefore, we believe that the model needs further development before being tested against observations.

6. TEST OF CORONAL HEATING MODELS

The scaling laws determined for the coronal heating rate in § 4 are used below to test whether the predictions of various coronal heating models (§ 5.2) are consistent with the observations. More precisely, we have deduced from soft X-ray observations and from the theory of quasi-static loops that the coronal heating has a power-law dependence on the mean magnetic flux density ($\bar{B}$). Indeed, we have deduced two pairs of power laws: from the temperature measurements ($\langle H_T \rangle_{\rm AR} \propto \bar{B}^{\widehat{HT}}$) and from the pressure measurements ($\langle H_P \rangle_{\rm AR} \propto \bar{B}^{\widehat{HP}}$) with both SXT and BCS data. In § 5.1 we have shown that the prediction of various coronal models can be transformed to a power law of $\bar{B}$ alone ($H_m \propto \bar{B}^{\widehat{Hm}}$). The goal is now to compare the prediction of $\widehat{Hm}$ for each coronal model with the two pairs of exponents ($\widehat{HT}$, $\widehat{HP}$) deduced from soft X-ray observations.

6.1. *Test Using SXT Data for the Long-Term Evolution of AR 7978*

The values of $\widehat{Hm}$ predicted by the different models with their error bars are shown in Figure 2 (models have error bars because L and N_e in eq. [29] are expressed as a function of $\bar{B}$ with the observational results). The horizontal lines in Figure 2 indicate the most probable values of $\widehat{HT}$ and $\widehat{HP}$, determined with SXT and the nonparametric fit. The shaded bands indicate the 90% confidence intervals. In order for a model to be strictly consistent with *Yohkoh* observations, its error bar must overlap with both bands. The most striking result from Figure 2 (*top left*; case *a*) is that only model 21 satisfies this criterion. It is worth noting that an error is present for model 21 in Figure 8 of Mandrini et al. (2000a): the exponent of B was set to 0 in the computa-

tion of the figure, while it should be 1 as written in their Table 5. If we acknowledge, however, that the error estimates are only approximate, we can conclude that models 2, 4, 5, 9, 11, 12, and 22 are marginally compatible with the observations. This conclusion holds for the entire coronal range of α [−2, 0.33]. The case $\alpha = -2$ is shown in Figure 2 (*bottom left*); in this case the confidence intervals of $\widehat{HT}$ and $\widehat{HP}$ do not overlap any longer. It is interesting to note in Figure 2 that the observations divide the stressing models (*top*) from the wave models (*bottom*), except in the case of models 21 and 22, which have indeed the same physics as models 8 and 12, respectively, but in which the footpoint motions are fast enough to produce waves.

Case *a* derives directly from the original heating models, which consider an almost uniform main magnetic field (both at the photospheric boundary and in the corona). However, van Ballegooijen (1986) pointed out that the concentration of the magnetic field in thin flux tubes at the photospheric level may have significant implications when twisting motions are involved (see § 5.1). The predictions of the models are then transformed to take into account this effect (case *b*). Figure 2 (*top right*), with $\alpha = 0$, shows that this has a significant effect on $\widehat{Hm}$ for several models. Three groups of models are within the 90% confidence interval of $\widehat{HT}$ and $\widehat{HP}$: models including a stochastic buildup of energy (models 1–3), models considering current layers (models 6–8), and some of the models using MHD turbulence (models 14 and 22). The only wave model that is compatible with SXT observations in case *b*, model 22, is indeed a model invoking turbulence; in this case the MHD turbulence is driven by waves, rather than by slow photospheric motions. Taking into account that in models invoking turbulence, the inertial and dissipation ranges do not depend on the driver, it is not surprising that the heating rate predicted by model 22 is similar to that of other turbulent models (in particular model 12). Model 5 (reconnection of the transverse field), model 9 (reconnection at X-points), and models 11–13 (MHD turbulence) are the next closest to the observations, although outside the error bars of both $\widehat{HT}$ and $\widehat{HP}$. In the extreme case $\alpha = -2$ (Fig. 2, *bottom right*), models 5 and 11–13 predict an exponent compatible, within the 90% confidence interval, with $\widehat{HP}$ (but not with $\widehat{HT}$, since it is not affected by α). We conclude that within the present uncertainties intrinsic to each model, the precise value of α is a relatively minor issue.

6.2. *Test Using SXT Data for Coronal Loops*

In a previous paper (Mandrini et al. 2000a), we have tested heating models combining the results of Klimchuk & Porter (1995) and Porter & Klimchuk (1995) on the scaling of temperature, pressure, and heating rate with the loop length in a set of nonflaring loops, with the results obtained on the scaling of the coronal field (deduced from photospheric extrapolations). Such an approach is more directly applicable to coronal heating models, which consider individual loops, and makes a more straightforward use of the thermal scaling laws (§ 2), since $T_{\max}$, N_e, and P_0 are directly measured. However, the error bars are large, and the method relies on the extrapolation of the photospheric field.

The approach presented here also lets us test coronal heating models that apply to individual loops, although it is most appropriate to models that consider the heating of larger regions (typically, a magnetic arcade; e.g., models 9, 10, 12, and 22). The two approaches are therefore complementary. In order to compare the results from these two approaches, we have transformed Figure 8 of Mandrini et al. (2000a) into Figure 3 using the relationship $L \propto \langle B \rangle_{\rm loop}^{-1/0.88}$ from the latter paper to express H_m as a function of $\langle B \rangle_{\rm loop}$ (a similar form to eq. [30]). This transformation includes the correction of model 21 mentioned above. In both cases *a* and *b*, the results of Figure 3 are fully compatible with the results of Figure 2. Although the two approaches represented by the figures share some common aspects (both use SXT observations and assume that loops are in thermal equilibrium), they are fundamentally independent of each other. It is therefore impressive that they give such similar results.

Our present approach also tests the coefficients *a–e* appearing in the models (eq. [29]) in a different way from Mandrini et al. (2000a). Rewriting their results as a function of B rather than of L, we find

$$H_m \propto B^{a-1.14b+1.09c} \tag{33}$$

for case *a*. With our approach, we obtain approximately

$$H_m \propto \bar{B}^{a-0.5b+c} \tag{34}$$

[for case *b* there is an additional term $-0.5(d+e)$ in the exponent, but it is the same in both studies]. Therefore, with

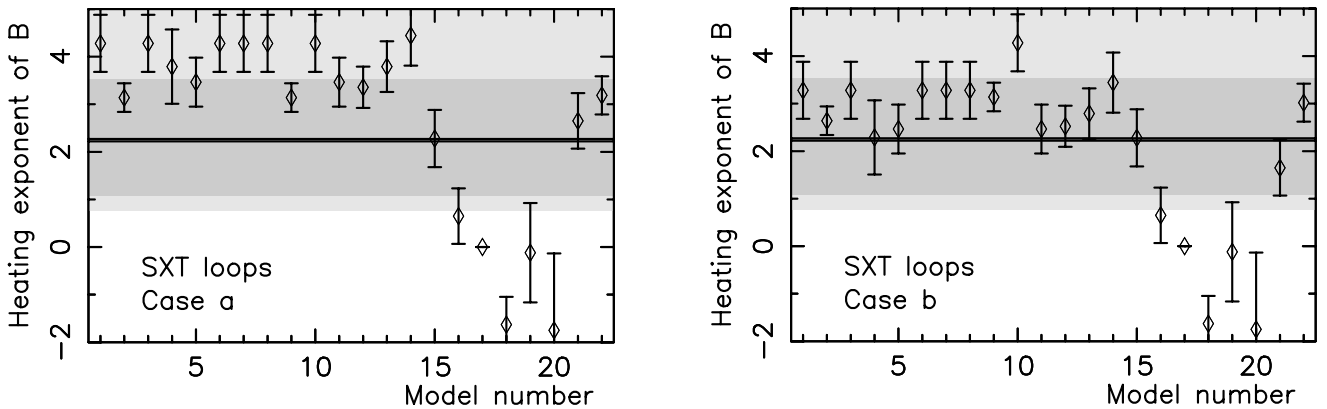

FIG. 3.—Same as Fig. 2, but with the observed scaling laws found by Porter & Klimchuk (1995) and Mandrini et al. (2000a) using SXT observations of coronal loops and magnetic field extrapolations. The law $L \propto \langle B \rangle_{\rm loop}^{-1/0.88}$, between the coronal loop length L and the mean coronal field $\langle B \rangle_{\rm loop}$ along the loops, has been used to transform the results of Mandrini et al. (2000a) to make them comparable to the results of the present study.

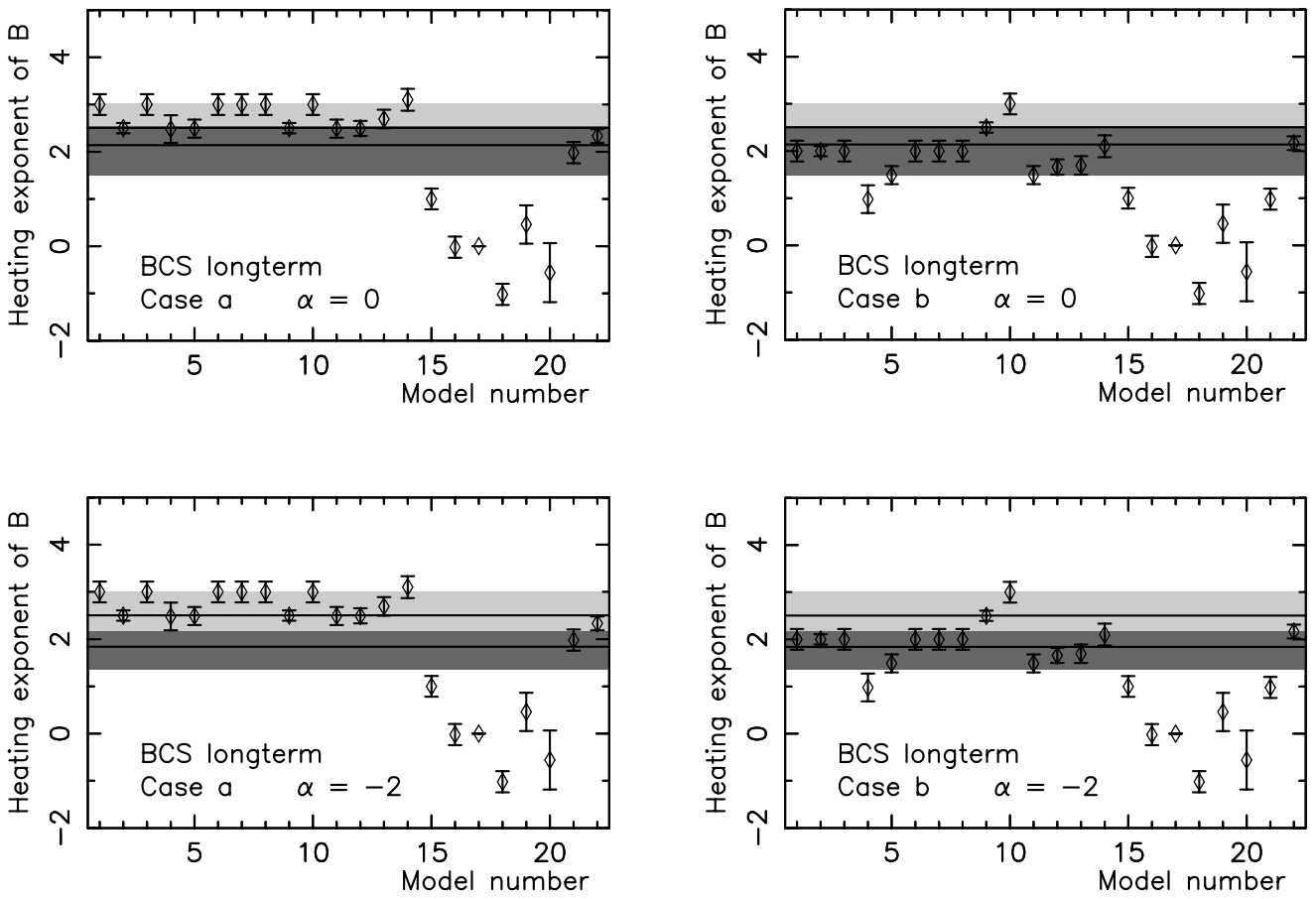

FIG. 4.—Same as Fig. 2, but using the results for the long-term evolution of AR 7978 obtained with BCS (§ 4.4, Table 2)

the present approach, the importance of the exponent of L, b, decreases in the heating rate expression. Because most models depend only weakly on the density (linked to the coefficient c), our approach puts more emphasis on testing the dependence of the models on the field strength than the approach of Mandrini et al. (2000a).

The long-term analysis of AR 7978 allows us to further constrain heating models because the error bars of the exponents are lower. This is due to the better representation of the data by a power law of $\bar{B}$ (lower dispersion) in our global approach (Fig. 5 of van Driel-Gesztelyi et al. 2003) than in the loop analysis of Porter & Klimchuk (their Figs. 1 and 2). This may happen at the expense of a larger bias in deriving the plasma parameters from global quantities ($\langle T \rangle_{\rm AR}$ and $\langle {\rm EM} \rangle_{\rm AR}$). There is a little evidence for this because the most probable values for the two exponents $\widehat{HT}$ and $\widehat{HP}$ are slightly different: 2.01 and 1.74 with SXT, $\alpha = 0$, and the nonparametric statistics (see comments in § 4). Moreover, these exponents are close to the most probable values derived by Mandrini et al. (2000a): 2.25 (using the transformation $L \propto \langle B \rangle_{\rm loop}^{-1/0.88}$, 0.88 being a mean value) and 2.04 (using the transformation $L \propto \langle B \rangle_{\rm loop}^{-1/0.97}$ as derived from averaging B along the field lines).

6.3. *Test Using BCS Data for the Long-Term Evolution of AR 7978*

The exponent $\widehat{HT}$ deduced from BCS is slightly higher than the one deduced from SXT, and the error bars are larger for both $\widehat{HT}$ and $\widehat{HP}$; thus, the results with BCS in case *a* are compatible with more models (see Fig. 4, *left*). Keeping the constraint that a model must be compatible with both $\widehat{HT}$ and $\widehat{HP}$, only the following models are left for $\alpha = 0$ (Fig. 4, *top left*): model 2 (stochastic buildup of energy with a critical angle), models 4 and 5 (magnetic reconnection), model 9 (reconnection at X-points), models 11–13 and 22 (MHD turbulence), and model 21 (current layers). With $\alpha = -2$ (Fig. 4, *bottom left*), only model 21 is compatible with both $\widehat{HT}$ and $\widehat{HP}$ as for SXT data.

For case *b* and $\alpha = 0$, the results (Fig. 4, *top right*) are the same as the ones found using SXT (Fig. 2, *top right*), except that the larger error bars and the shift in $\widehat{HT}$ ($=2.51^{+0.52}_{-0.51}$) allow model 9 to also be compatible with both BCS observations. The larger error bars with BCS mask the effect of α compared to SXT results: for example, the results for $\alpha = 0$ and $\alpha = -2$ are similar (compare Fig. 4 top right with bottom right).

One of the stressing models, model 10 (Taylor relaxation), lies outside the error bars of both SXT and BCS data (it is only marginally compatible with $\widehat{HT}$ for BCS). Such a model assumes that the magnetic field would relax to a minimum energy state (i.e., linear force-free field), preserving the magnetic helicity. Magnetic extrapolations of MDI data, using a linear force-free approach, were compared with the SXT loops; the results show that AR 7978 had a moderate gradient of the magnetic shear throughout its lifetime, in particular between the north and the south portion of the AR (van Driel-Gesztelyi et al. 1999; Mandrini et al. 2000b).

Moreover, AR 7978 had numerous coronal mass ejections during its lifetime, which have a fundamental impact on the magnetic helicity budget of the AR (Démoulin et al. 2002), implying that AR 7978 did not evolve with a constant magnetic helicity, even after the emergence phase was over. Therefore, we think that the relaxation to a linear force-free field is not completed during the lifetime of the AR.

6.4. *Comparison with Other Results*

Since our previous work (Mandrini et al. 2000a), two other studies (Foley et al. 2002; Schrijver & Aschwanden 2002) have tested coronal heating models. The latter papers use very different approaches from both Mandrini et al. (2000a) and this study. It is then remarkable that the four works point to the same set of models as the most plausible to explain the coronal heating mechanism. This certainly strengthens the results of each of them and indicates which models need to be further developed (or seriously revised).

Foley et al. (2002) studied the temperature gradient in the core of coronal streamers using the Coronal Diagnostic Spectrometer on board *SOHO*. They assumed that the divergence of the conductive flux is proportional to the heating (eq. [21]) and compared the observational results obtained for solar minimum and maximum. They concluded that stressing models based on reconnection or MHD turbulence best fit their observations. It is noteworthy that they studied much larger coronal structures than we have, since they analyzed coronal streamers that extend up to 2.3 $R_\odot$. This is an indication that the same heating mechanism can be at work at relatively small scales (coronal loops), as well as on large scales (of the order of 1 $R_\odot$).

Schrijver & Aschwanden (2002) have carried out an extensive simulation of the coronal emission of the Sun and cool stars (the latter with a magnetic flux emergence rate up to 30 times larger than the solar case). They simulated the full star photospheric field and used a potential field approximation for the coronal field. Then, they used Serio et al. (1981) scaling laws to compute the X-ray emission during the activity cycle. Exploring the space of parameters and considering solar and stellar constraints, they concluded that the most likely candidates are heating via the dissipation of current layers and/or MHD turbulence. Apart from the thermal scaling laws and the *Yohkoh*/SXT observations (used in a different way than we do), this study has no common base with our present work; nevertheless, the results are similar.

7. CONCLUSION

Models of coronal heating usually predict a volumetric heating rate H_m, which depends on several parameters (one of them being the coronal magnetic field strength) as a power law (see eq. [29]). Because of the simple bipolar nature of AR 7978 and the absence of other significant nearby flux concentration, the photospheric flux density $\bar{B}$ is a measure of the mean coronal magnetic field of this AR. Van Driel-Gesztelyi et al. (2003) have found a power-law relationship between the mean coronal plasma parameters and $\bar{B}$. With these results we can transform the predictions of the models to power laws of $\bar{B}$ alone ($H_m \propto \bar{B}^{\widehat{Hm}}$). On the other hand, the restriction to quiet phases of the AR allows us to use the thermal scaling laws obtained previously by several authors (see § 2) and to derive two estimates of the coronal heating dependence: $\langle H_T \rangle_{\rm AR} \propto \bar{B}^{\widehat{HT}}$ and $\langle H_P \rangle_{\rm AR} \propto \bar{B}^{\widehat{HP}}$ (see § 4.2). The objective of the present study is to compare the values of $\widehat{Hm}$ predicted by various models with the values of $\widehat{HT}$ and $\widehat{HP}$ deduced from the observations.

One of the scaling laws (eq. [5]) lets us test whether the hypotheses we have made are valid. We have found only a slight deviation from this scaling (see §§ 3.2 and 3.3). However, this deviation has only minor importance in testing current coronal heating models, since, in particular, the models are so much idealized that they can only predict an estimate for the exponent $\widehat{Hm}$. More precisely, the small deviation from the scaling law of equation (5) introduces a slight difference in the exponents $\widehat{HT}$ and $\widehat{HP}$. The difference between $\widehat{HT}$ and $\widehat{HP}$ is indeed lower than the uncertainty we have on the exponent $\widehat{Hm}$ for each model (e.g., the difference between cases *a* and *b*; see Figs. 2 and 4, comparing the left-hand and right-hand sides).

The long-term study of AR 7978 gives consistent results between SXT and BCS for $\widehat{HP}$ and $\widehat{HT}$, within the confidence interval of both normal and nonparametric fits (Fig. 1). This strengthens our conclusions, since the very different nature of the instruments implies that probable intrinsic biases should be different.

It is noteworthy that the values derived differently for both exponents $\widehat{HP}$ and $\widehat{HT}$ are very close to 2. This implies that the heating rate per unit volume is simply proportional to the coronal magnetic energy density (when it is expressed only as a function of the magnetic field strength)!

Our study confirms the results of Mandrini et al. (2000a): models involving the gradual stressing of the coronal magnetic field by slow footpoint motions are in better agreement with the observational constraints of both SXT and BCS than models involving MHD waves injected at the base of the corona (the only wave models compatible with the data are the two models that have a counterpart in the stressing models). The lower error bars obtained with the long-term study of AR 7978 allow us to further constrain heating models.

If we use the original scaling laws as derived assuming that the magnetic field does not flare out above photospheric flux concentrations (case *a*), then SXT results exclude all models except wave model 21, while BCS results are compatible with several models. However, if we take into account the observed fact that the photospheric field is concentrated in thin flux tubes (case *b*), then both the SXT and BCS results are compatible, within a 90% confidence interval, with three groups of models: models considering a stochastic buildup of energy (models 1–3), models including current layers (models 6–8), and models implying MHD turbulence (models 12–14 and 22). This result agrees with the independent result of Schrijver & Aschwanden (2002) that constrains the heating mechanisms by comparing the modeling of the X-ray emission of the Sun and cool stars with observations.

Indeed, the three groups of retained models have some physics in common. Milano et al. (1999) have shown, through an MHD simulation of two flux tubes formed by twisting motions, that turbulence develops when reconnection takes place between them. It is then not surprising that the scaling laws of the three groups of models are so close. The slight differences in their scaling may only reflect the approximations considered when attacking the same physical problem from very different points of view.

The agreement of the results obtained with three separate approaches (SXT measurements of coronal loops and long-

term study of an AR with two very different instruments, SXT and BCS) shows that the scaling law analysis is a useful tool for obtaining information on the coronal heating mechanism. With this analysis, error bars can be reduced enough to distinguish between mechanisms that are physically different. Indeed, each heating model needs to be refined, in particular to include a more realistic AR-like magnetic configuration; considering only the magnetic field concentration at the photosphere implies a larger variation in the exponent predicted ($\widehat{Hm}$) than the error bars of the observations.

We thank the referee, Giovanni Peres, for constructive comments on the paper. The authors thank the *SOHO*/MDI consortium for the *SOHO* data and the Mullard Space Science Laboratory (MSSL) Solar UK Research Facility for *Yohkoh* data. *SOHO* is a joint project by ESA and NASA. P. D. and C. H. M. acknowledge financial support from ECOS (France) and SECyT (Argentina) through their cooperative science program (A01U04). L. v. D.-G. was supported by research fellowship F/02/035 of the Katholieke Universiteit Leuven and by Hungarian government grants OTKA T-038013 and T-032846. P. D. and L. v. D.-G. acknowledge the Hungarian-French Science and Technology cooperative program. C. H. M. is grateful for an MSSL, University College London (UCL), visitor's grant. The work of J. A. K. was supported by NASA and the Office of Naval Research. P. D., L. v. D.-G., and L. K. H. acknowledge travel support from the Royal Society Joint Project (MSSL/UCL–Observatoire de Paris, Meudon). L. K. H. is grateful to PPARC for the award of an advanced fellowship.

APPENDIX

EXPONENTS OF POWER LAWS

We give here a concise definition of every power law used, including a reference to the section in which it is first introduced.

1. Exponents coming from the theory of coronal loops:

a) The exponent α (§ 2.2) in the optically thin radiative loss function $\Lambda(T) \propto T^{\alpha}$ (where T is the coronal temperature).
b) Two power-law expressions for the average-loop heating (§§ 2.2 and 4.2) from the theory of quasi-static loops:

$$\langle H \rangle_{\rm loop} \propto P_0^{14/(11-2\alpha)} L^{-4(2-\alpha)/(11-2\alpha)} , \tag{A1}$$

$$\langle H \rangle_{\rm loop} \propto T_{\rm max}^{7/2} L^{-2} , \tag{A2}$$

where $T_{\rm max}$ is the maximum temperature, P_0 the plasma pressure at the loop base, and L the loop half-length.

2. Exponents deduced from soft X-rays and magnetic field observations:

a) The exponents $\hat{T}$, $\hat{N}$, and $\hat{P}$ (§ 3.1) of the mean temperature $\langle T \rangle_{\rm AR}$, electron density $\langle N_e \rangle_{\rm AR}$, and pressure $\langle P \rangle_{\rm AR}$ with the magnetic flux density $\bar{B}$ (van Driel-Gesztelyi et al. 2003):

$$\langle T \rangle_{\rm AR} \propto \bar{B}^{\hat{T}} , \qquad \langle N_e \rangle_{\rm AR} \propto \bar{B}^{\hat{N}} , \qquad \langle P \rangle_{\rm AR} \propto \bar{B}^{\hat{P}} .$$

b) The exponent $\hat{A}$ (§ 3.1) of the AR magnetic area with $\bar{B}$:

$$A \propto \bar{B}^{\hat{A}} .$$

The length of the coronal loops is supposed to scale as $L \propto \sqrt{A} \propto \bar{B}^{\hat{A}/2}$.

3. Exponents of the heating rate deduced by combining observations and the theory of coronal loops:

a) The exponent $\widehat{HT}$ (§ 4.2) of the average heating deduced from equation (A2):

$$\langle H_T \rangle_{\rm AR} \propto \bar{B}^{\widehat{HT}} .$$

b) The exponent $\widehat{HP}$ (§ 4.2) of the average heating deduced from equation (A1):

$$\langle H_P \rangle_{\rm AR} \propto \bar{B}^{\widehat{HP}} .$$

4. Exponents from theoretical heating models:

a) Exponents a, b, c, d, and e (§ 5.1), defined by each theoretical model of coronal heating:

$$H_m \propto B^a L^b N_e^c V^d R^e .$$

b) The exponent $\widehat{Hm}$ (§ 5.1) of a theoretical model when the heating is expressed only as a function of the magnetic flux density $\bar{B}$:

$$H_m \propto \bar{B}^{\widehat{Hm}} .$$

REFERENCES

Aly, J. J., & Amari, T. 1997, A&A, 319, 699
Aschwanden, M. J., Schrijver, C. J., & Alexander, D. 2001, ApJ, 550, 1036
Aschwanden, M. J., et al. 2000, ApJ, 531, 1129
Berger, M. A. 1991, A&A, 252, 369
———. 1993, Phys. Rev. Lett., 70, 705
Browning, P. K., & Priest, E. R. 1986, A&A, 159, 129
Cargill, P. J., & Klimchuk, J. A. 1997, ApJ, 478, 799
Chiuderi, C., Einaudi, G., & Torricelli-Ciamponi, G. 1981, A&A, 97, 27
Cook, J. W., Cheng, C.-C., Jacobs, V. L., & Antiochos, S. K. 1989, ApJ, 338, 1176
Craig, I. J. D., McClymont, A. N., & Underwood, J. H. 1978, A&A, 70, 1
Culhane, J. L., et al. 1991, Sol. Phys., 136, 89
Démoulin, P., Mandrini, C. H., van Driel-Gesztelyi, L., Thompson, B., Plunkett, P., Kővári, Zs., Aulanier, G., & Young, A. 2002, A&A, 382, 650
Dmitruk, P., & Gómez, D. O. 1997, ApJ, 484, L83
Einaudi, G., Velli, M., Politano, H., & Pouquet, A. 1996, ApJ, 457, L113
Foley, C. R., Patsourakos, S., Culhane, J. L., & MacKay, D. 2002, A&A, 381, 1049
Galsgaard, K., & Nordlund, Å. 1996, J. Geophys. Res., 101, 13445
———. 1997, J. Geophys. Res., 102, 219
Halberstadt, G., & Goedbloed, J. P. 1995, A&A, 301, 559
Hara, H., Tsuneta, S., Lemen, J. R., Acton, L. W., & McTierman, J. M. 1992, PASJ, 44, L135
Hendrix, D. L., Van Hoven, G., Mikić, Z., & Schnack, D. D. 1996, ApJ, 470, 1192
Heyvaerts, J., & Priest, E. R. 1984, A&A, 137, 63
———. 1992, ApJ, 390, 297
Hollweg, J. V. 1985, in Advances in Space Plasma Physics, ed. B. Buti (Singapore: World Scientific), 77
Inverarity, G. W., & Priest, E. R. 1995a, A&A, 296, 395
———. 1995b, A&A, 302, 567
Inverarity, G. W., Priest, E. R., & Heyvaerts, J. 1995, A&A, 293, 913
Kano, R., & Tsuneta, S. 1995, ApJ, 454, 934
———. 1996, PASJ, 48, 535
Klimchuk, J. A. 2000, Sol. Phys., 193, 53
Klimchuk, J. A., & Cargill, P. J. 2001, ApJ, 553, 440
Klimchuk, J. A., & Porter, L. J. 1995, Nature, 377, 131
Landi, E., & Landini M. 1999, A&A, 347, 401
Mackay, D. H., Galsgaard, K., Priest, E. R., & Foley, C. R. 2000, Sol. Phys., 193, 93
Mandrini, C. H., Démoulin, P., & Klimchuk, J. A. 2000a, ApJ, 530, 999
Mandrini, C. H., van Driel-Gesztelyi, L., Thompson, B., Plunkett, S., Démoulin, P., & Aulanier, G. 2000b, Int. Geophys., 39(1), 73
Milano, L. J., Dmitruk, P., Mandrini, C. H., Gómez, D., & Démoulin, P. 1999, ApJ, 521, 889
Milano, L. J., Gómez, D. O., & Martens, P. C. H. 1997, ApJ, 490, 442
Ofman, L., Davila, J. M., & Steinolfson, R. S. 1995, ApJ, 444, 471
Orlando, S., Peres, G., & Serio, S. 1995a, A&A, 294, 861
———. 1995b, A&A, 300, 549
Parker, E. N. 1983, ApJ, 264, 642
———. 1988, ApJ, 330, 474
Peres, G. 2000, Sol. Phys., 193, 33
Pevtsov, A. A., & Acton, L. W. 2001, ApJ, 554, 416
Porter, L. J., & Klimchuk, J. A. 1995, ApJ, 454, 499
Reale, F. 2002, ApJ, 580, 566
Roald, C. B., Sturrock, P. A., & Wolfson, R. 2000, ApJ, 538, 960
Rosner, R., Tucker, W. H., & Vaiana, G. S. 1978, ApJ, 220, 643
Ruderman, M. S., Berghmans, D., Goosens, M., & Poedts, S. 1997, A&A, 320, 305
Scherrer, P. H., et al. 1995, Sol. Phys., 162, 129
Schrijver, C. J., & Aschwanden, M. J. 2002, ApJ, 566, 1147
Serio, S., Peres, G., Vaiana, G. S., Golub, L., & Rosner, R. 1981, ApJ, 243, 288
Sturrock, P. A., Roald, C. B., & Wolfson, R. 1999, ApJ, 524, L75
Sturrock, P. A., & Uchida, Y. 1981, ApJ, 246, 331
Taylor, J. B. 1974, Phys. Rev. Lett., 33, 1139
Testa, P., Peres, G., Reale, F., & Orlando, S. 2001, in Proc. First Solar Orbiter Workshop: Solar Encounter, ed. B. Battrick & H. Sawaya-Lacoste (ESA SP-493; Noordwijk: ESA), 389
———. 2002, ApJ, 580, 1159
Tsuneta, S., et al. 1991, Sol. Phys., 136, 37
van Ballegooijen, A. A. 1986, ApJ, 311, 1001
van Driel-Gesztelyi, L. 1998, in ASP Conf. Ser. 155, Three-Dimensional Structure of Solar Active Regions, ed. C. Alissandrakis & B. Schmieder (San Francisco: ASP), 202
van Driel-Gesztelyi, L., Démoulin, P., Mandrini, C. H., Harra, L., & Klimchuk, J. A. 2003, ApJ, 586, 579
van Driel-Gesztelyi, L., et al. 1999, in ASP Conf. Ser. 184, Magnetic Fields and Oscillations, ed. B. Schmieder, A. Hofmann, & J. Staude (San Francisco: ASP), 302
Vekstein, G. E., Priest, E. R., & Steele, C. D. C. 1993, ApJ, 417, 781
Vesecky, J. F., Antiochos, S. K., & Underwood, J. H. 1979, ApJ, 233, 987
Watko, J. A., & Klimchuk, J. A. 2000, Sol. Phys., 193, 77
Wheatland, M. S., Sturrock P. A., & Acton, L. W. 1997, ApJ, 482, 510
Winebarger, A. R., Warren, H. P., & Mariska, J. T. 2003, ApJ, in press
Yashiro, S., & Shibata, K. 2001, ApJ, 550, L113